Electronic Supplementary Material (ESI) for Nanoscale.
This journal is © The Royal Society of Chemistry 2018

Supporting Information

On-surface synthesis: a promising strategy toward the encapsulation of air unstable ultra-thin 2D materials

Qiang Li,† [a] *Yinghe Zhao,*† [a] *Jiyuan Guo,*[a,b] *Qionghua Zhou,*[a] *Qian Chen*[a] *and Jinlan Wang**[a,c]

[a]School of Physics, Southeast University, Nanjing 211189, China

[b]Department of Physics, Jiangsu University of Science and Technology, Zhenjiang 212003, China

[c]Synergetic Innovation Center for Quantum Effects and Applications (SICQEA), Hunan Normal University, Changsha 410081, China

†These authors contributed equally to this work.

Corresponding Author

E-mail: jlwang@seu.edu.cn

Table of Contents

1. Computational details

DFT Calculations: All DFT calculations are implemented in the Vienna *ab initio* simulation package with vdW modification (D2).[1, 2] The exchange-correlation functional is based on Perdew-Burke-Ernzerhof (PBE) generalized gradient approximation.[3] The interaction between electron and ion is described by the projector augmented wave potential. The kinetic energy cutoff are set to be 400 eV. All structures are fully relaxed until the atomic forces on each atom are smaller than 0.02 eVÅ^{-1} and the total energy change is less than 1.0×10^{-4} eV.

MD Simulations: All MD simulations are performed using Gromacs-4.5.4 package built on all-atom AMBER99SB[15] and Universal[16] force field, together with SPCE model.[4-7] The simulations are carried out in the canonical ensemble (number of molecules, volume, and temperature are constant) with a time step of 1 fs. Intermolecular interactions are described by combing the vdW and electrostatic interactions that are calculated according to 12-6 Lennard-Jones potential and Coulomb's law with a spherical cut-off of 1.5 nm. Outside 1.5 nm, the smoothed particle mesh Ewald sum is employed to deal with the electrostatic interaction.[8] The temperature is controlled by means of the Berendsen thermostat, and periodic boundary conditions are employed to avoid the edge effect.

AIMD Simulations: We perform AIMD simulations based on DFT using the cp2k code.[9, 10] The entire system is treated quantum-mechanically, representing valence and core electrons with double-ζ basis sets of the MOLOPT type and Goedecker−Teter−Hutter pseudopotentials, respectively.[11, 12] The D3 method by Grimme is used to account for dispersion interactions in an approximate way.[13] The time step is fixed at 0.5 fs and the temperature maintained at 300 K using a Nosé–Hoover thermostat chain.

2. Organic molecule layers

As shown in Figure S1 below, the intermolecular distance changes in a range of 2.4-3.4 Å. The molecules can connect closely with hydrogen bonding, but the molecules can also be far away from each other with very weak H…H interactions, where active species of oxygen and water can pass through.

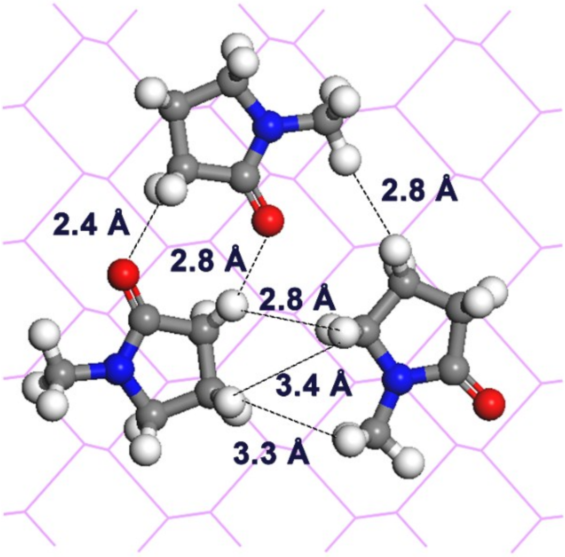

Figure S1. Optimized three NMP molecules on the surface of BP.

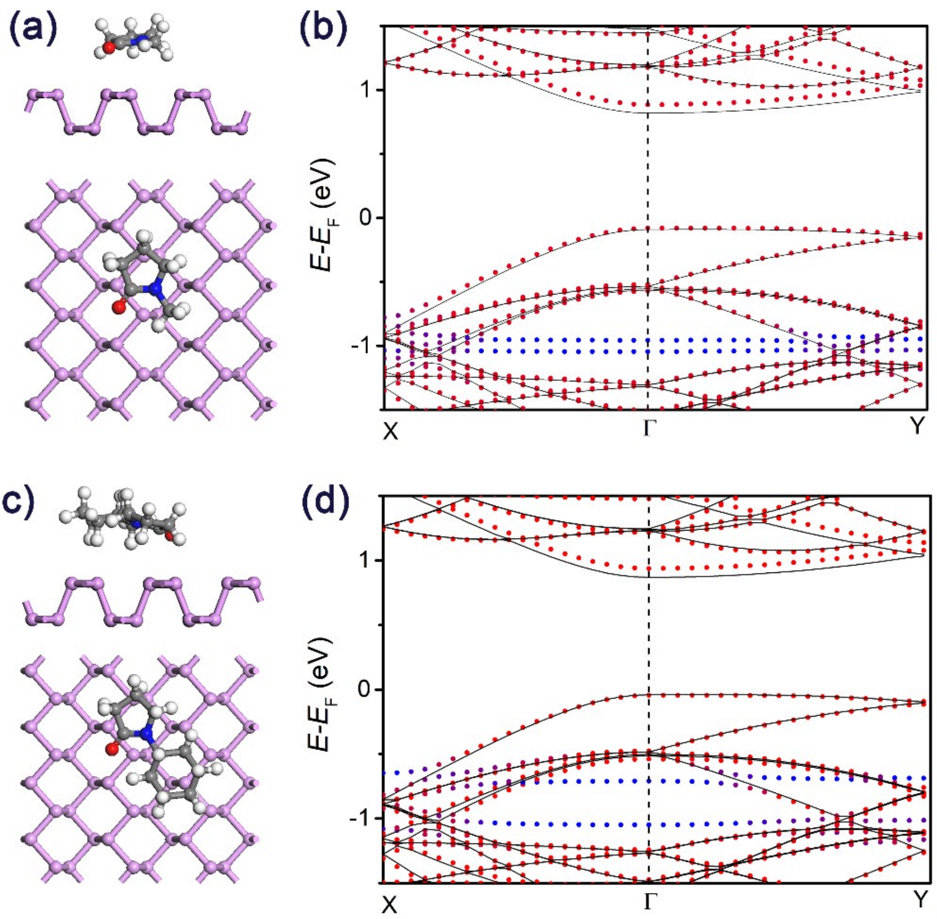

Figure S2. a) Top and side views of NMP on BP surface; b) Calculated band structures of the pristine BP (gray solid line) and the NMP-adsorbed BP (red and blue dotted lines) where red and blue lines record the contributions of BP and NMP, respectively; c) Top and side views of CHP on BP surface; d) Calculated band structures of the pristine BP (gray solid line) and the CHP-adsorbed BP (red and blue dotted lines) where red and blue lines record the contributions of BP and CHP, respectively.

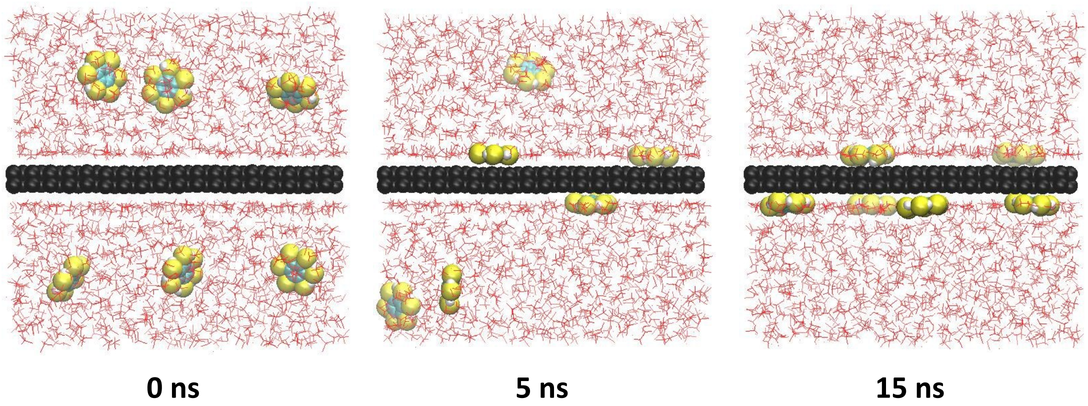

Figure S3. Snapshots from MD simulation of BHT molecules dispersion (with a more disturbed patter comparing with the case in Figure1) in the CH_2Cl_2 solvent in the presence of BP.

3. 2D coordination polymers

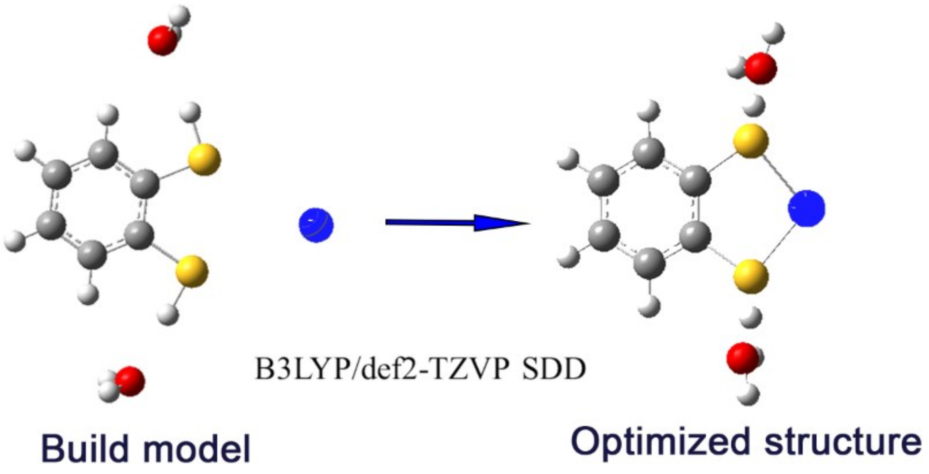

Figure S4. Initial and optimized structures of Cu^{2+} attaching a BHT molecule with two H_2O around.

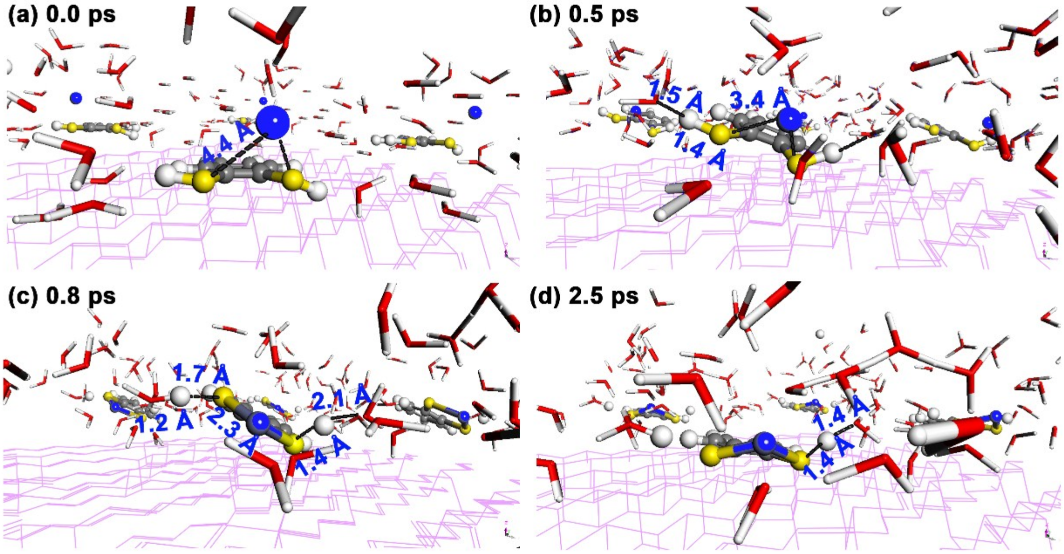

Figure S5. a-d) Snapshots from the AIMD trajectory simulating the breaking of S-H bonds and formation of Cu-S bonds.

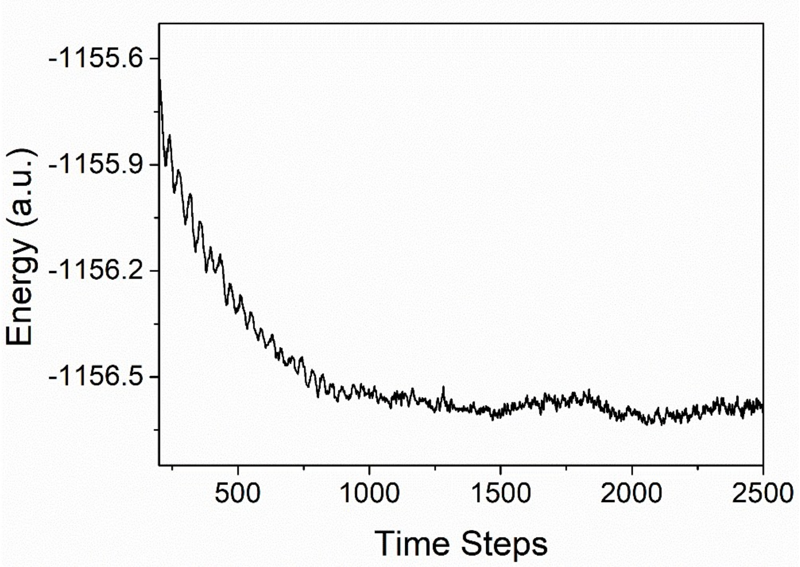

Figure S6. Energy fluctuation with AIMD time steps of 0.5 ps.

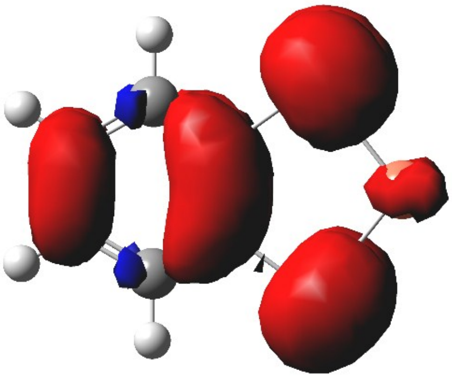

Figure S7. Spin density of Cu-BHT molecule, and the density is mostly distributed on two S atoms.

4. Electronic calculations of heterostructures

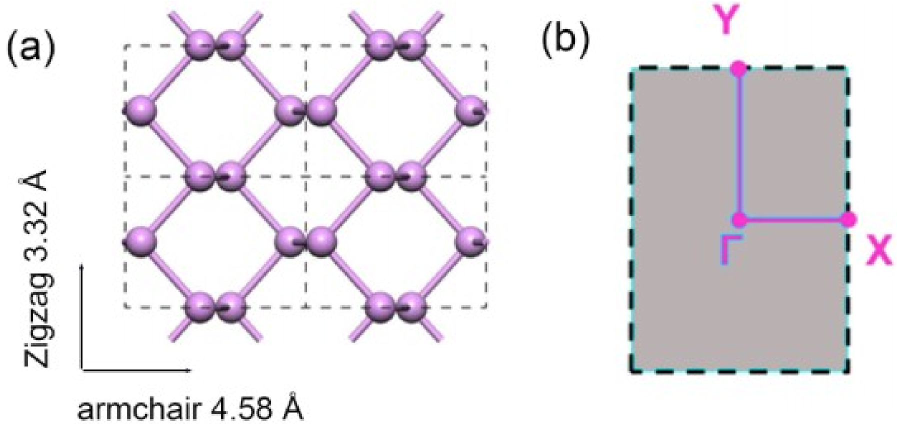

Figure S8. a) Top view of the atomic structure of BP monolayer and b) the associated Brillouin zone.

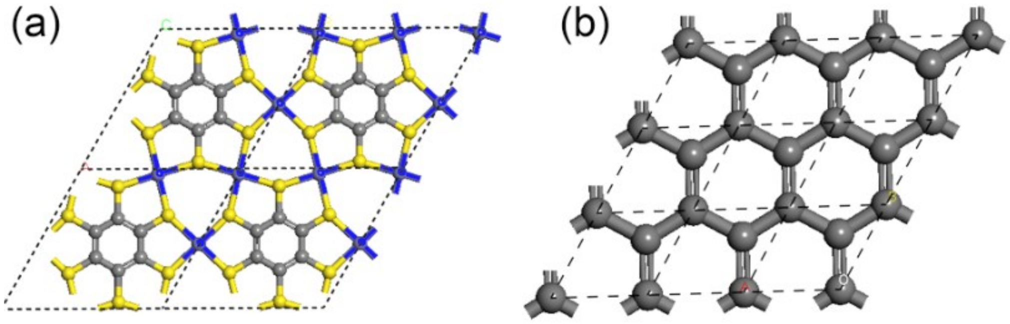

Figure S9. a&b) Top view of the optimized atomic structure of CuBHT and graphene monolayers, where a=b=8.80 Å for CuBHT polymer and a=b=2.46 Å for graphene.

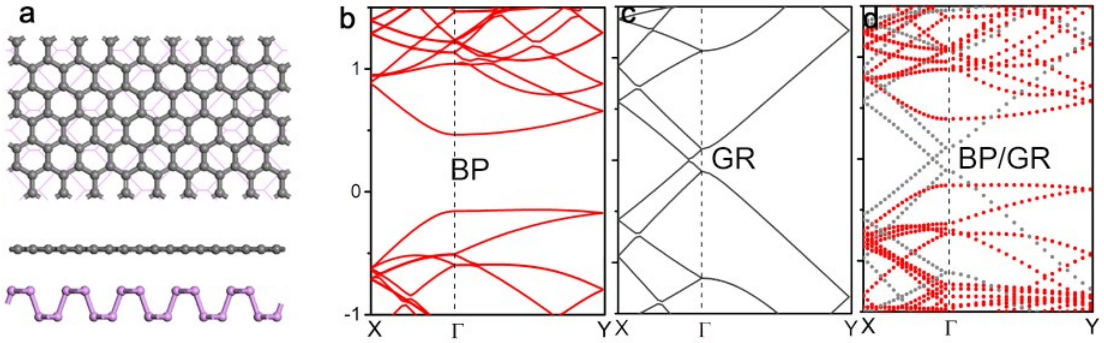

Figure S10. a) Top and side views of BP/graphene hetrostructure; b-d) Band structures of monolayer BP, monolayer graphene, and BP/graphene bilayer.

As we see from Figure S8 and Figure S9, CuBTH/graphene and BP belong to different crystal systems with significantly different lattice parameters, where hexagonal P63/mmc for CuBHT/graphene and orthorhombic D$_2$h for BP, respectively. To obtain the associated interface supercells, we have defined orthorhombic graphene unit cells from $\sqrt{3} \times 1$ primitive unit cell, and afterward we created a 9 × 3 supercell for overlapping BP supercell with size of 5 × 4. For CuBHT, we have defined orthorhombic CuBTH unit cells from $\sqrt{3} \times 1$ primitive CuBTH units, and afterward we created a 2 × 1 supercell for overlapping BP supercell with size of 9 × 2. The overall induced strain in the lattice is <4%, which would induce the difference of BP band structures as we see in Figure 3 &S10.

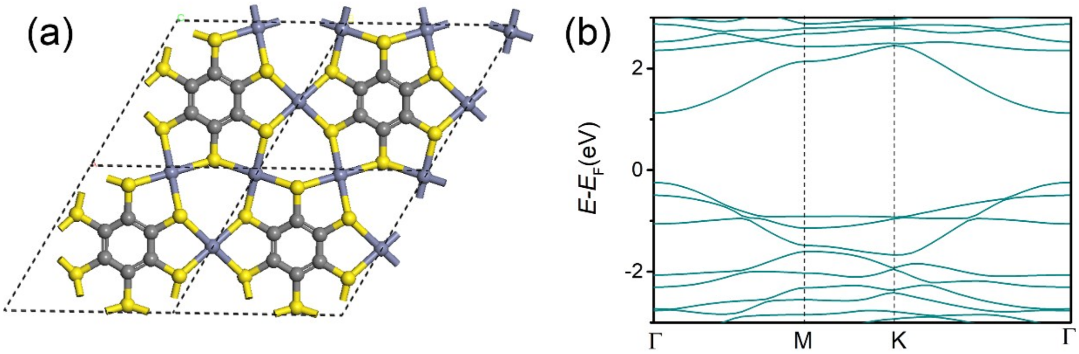

Figure S11. a) Top view of the atomic structure of ZnBHT monolayer and b) the associated band structure, which shows a direct band gap of 1.36 eV at gamma point.

5. GaSe

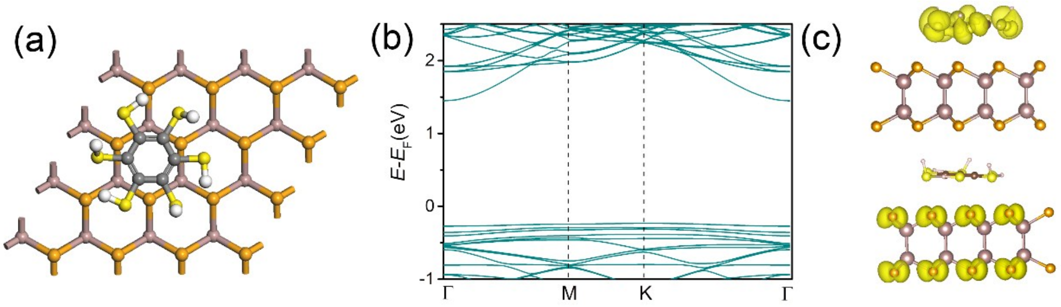

Figure S12. a) Top view of the atomic structure of BHT molecule adsorption on GaSe surface; b) The associated band structure; c) Partial charge densities of the VBM and CBM.

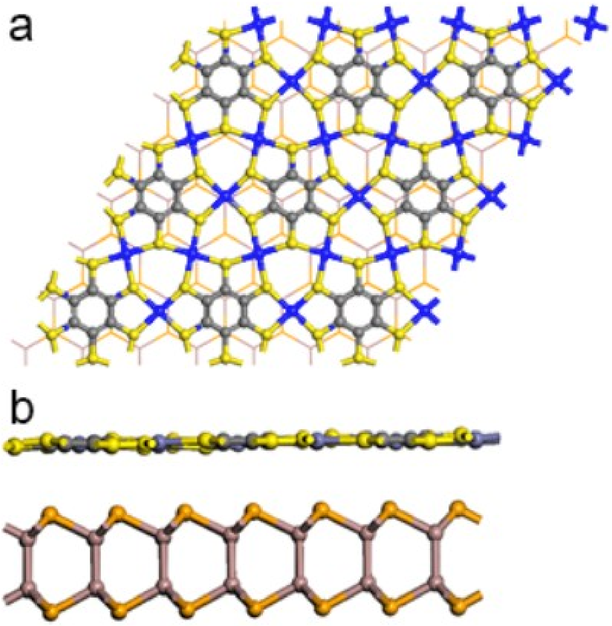

Figure S13. Top (a) and side (b) view of supercell structure that used for electronic structure calculation of GaSe/CuBHT, which corresponds to a size of 7 × 3.

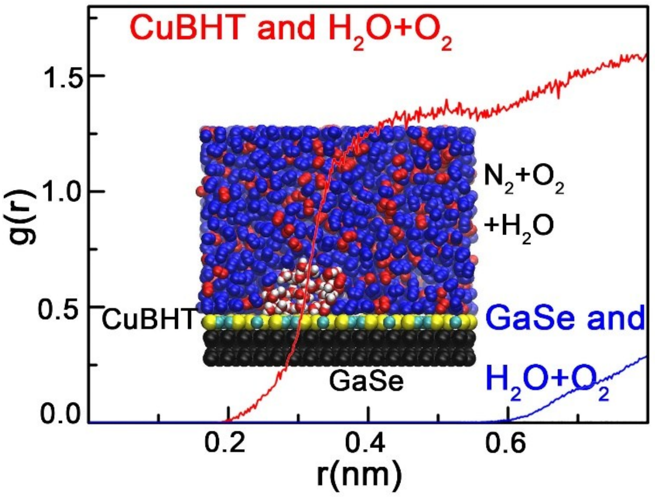

Figure S14. Radial distribution function of the O_2/H_2O on the surface of GaSe/CuBHT heterostrcture after evolution of the system after 30 ns.

6. References

1. G. Kresse and J. Furthmüller, *Phys. Rev. B*, 1996, **54**, 11169-11186.
2. S. Grimme, *J. Comput. Chem.*, 2006, **27**, 1787-1799.
3. J. P. Perdew, K. Burke and M. Ernzerhof, *Phys. Rev. Lett.*, 1996, **77**, 3865-3868.
4. E. J. Sorin and V. S. Pande, *Biophys. J.*, 2005, **88**, 2472-2493.
5. B. Hess, C. Kutzner, D. van der Spoel and E. Lindahl, *J. Chem. Theory Comput.*, 2008, **4**, 435-447.
6. Andrew T. Guy, Thomas J. Piggot and S. Khalid, *Biophys. J.*, 2012, **103**, 1028-1036.
7. A. K. Rappe, C. J. Casewit, K. S. Colwell, W. A. Goddard and W. M. Skiff, *J. Am. Chem. Soc.*, 1992, **114**, 10024-10035.
8. U. Essmann, L. Perera, M. L. Berkowitz, T. Darden, H. Lee and L. G. Pedersen, *J. Chem. Phys.*, 1995, **103**, 8577-8593.
9. *CP2K developers group under the terms of theGNUGeneral Public Licence 2015 see* www.cp2k.org.
10. J. VandeVondele, M. Krack, F. Mohamed, M. Parrinello, T. Chassaing and J. Hutter, *Comput. Phys. Commun.*, 2005, **167**, 103-128.
11. J. VandeVondele and J. Hutter, *J. Chem. Phys.*, 2007, **127**, 114105.
12. S. Goedecker, M. Teter and J. Hutter, *Phys. Rev. B*, 1996, **54**, 1703-1710.
13. S. Grimme, J. Antony, S. Ehrlich and H. Krieg, *J. Chem. Phys.*, 2010, **132**, 154104.